Supplemental Material

Figures S1–S3

Videos S1–S4.

Supplemental Dataset S1. EDX analyses of minerals in the matrix and pores are compiled in.

Supplemental Material

A synkinematic origin of the SSMPs?

Interpreting the origin of SSMPs requires the establishment of the timing of their formation: are they synkinematic or post-kinematic? Hypothetically, a younger deformational and/or metamorphic overprint, weathering or sample-preparation could have altered the sample after the mylonitic deformation. We found no evidence for either of these:

- The mylonitic deformation was the last pervasive deformation event affecting the rocks in the Cala Serena (Carreras, 2001, Fusseis et al., 2006).

- The sample shows no obvious signs of retrogression, disintegration or weathering, for which Bt and feldspars would be excellent indicators. Bt reacts to Chl and Ab during retrogression (Ferry, 1985) and weathers to Vrm or Kln (Wilson, 2004). Both Bt generations in the sample appear stable and neither Chl nor any clay minerals were found in any significant quantities. Secondary Ab is abundant in the sample, but is associated with the synkinematic consumption of Ab1. Where Ab weathers, it forms Sme, halloysite and Kln, often via internal dissolution of feldspars, and occasionally via the formation of a rim depleted in cations (Wilson, 2004), neither of which were found around Ab1 clasts, nor were clay minerals found anywhere in the sample.

- In weathering, access to meteoric water via a percolating network of pores and fractures is critical (Meunier et al., 2007). No such network exists in the sample. Our μCT data, which image the pores in a non-invasive, non-destructive way, demonstrate that the SSMPs appear isolated and are generally not connected to any postmylonitic fractures or other potential fluid pathways that could have facilitated the dissolution and selective leaching of minerals from specific strain shadows. The non-invasive imaging also precludes that sample preparation caused the observed porosity.

- The compositionally very similar host rock in the immediate proximity of the shear zone (<1 m away), which shows no mylonitic overprint but would have experienced the same retrogression and weathering, does not exhibit SSMPs (Suppl. Fig. 1).

These arguments allow us to interpret the SSMPs in the synkinematic context of the processes that define the ultramylonite.

Ferry, J.M., 1985, Hydrothermal alteration of Tertiary igneous rocks from the Isle of Skye, northwest Scotland: II. Granites: Contributions to Mineralogy and Petrology, v. 91, p. 283–304, https://doi.org/10.1007/BF00413353.

Meunier, A., Sardini, P., Robinet, J.C., and Prêt, D., 2007, The petrography of weathering processes: Facts and outlooks: Clay Minerals, v. 42, p. 415–435,

https://doi.org/10.1180/claymin.2007.042.4.01.

Wilson, M.J., 2004, Weathering of the primary rock-forming minerals: Processes, products and rates: Clay Minerals, v. 39, p. 233–266, https://doi.org/10.1180/0009855043930133.

**Image Analysis / Method Summary:**

The backscatter electron (BSE) mosaic formed the basis of a detailed analysis of the SSMPs. Some SEM images are composed of 50% BSE and 50% SE signal (Fig. 2). In BSE images, porosity appears black.

To quantify volumes and examine the shape of the SSMPs non-invasive, high-quality, high-resolution synchrotron X-radiation microtomography data of the ultramylonite and its protolith were collected. These datasets were produced with the monochromatic x-ray beam at the TOMCAT beamline of the Swiss Light Source. The samples were mounted onto a rotary stage, where data was collected in 0.25° increments over 180°. The minimum effective pixel size achieved was 0.65 μm to give 0.65 x 0.65 x 0.65 μm3 voxels for three-dimensional rendering of volumes. Virtual representations of the samples were reconstructed from the image projections using gridrec implemented in TOMCAT's in-house reconstruction workflow. The adsorption microtomographic

data resolve the different minerals in the sample well and clearly highlight the pores, which attenuate the least and appear darkest in the microtomographs.

Porosity in both datasets was segmented using a random forest classifier implemented in the WEKA segmentation tool in FIJI. The resulting probability maps were thresholded to a probability of 80% to account for uncertainties in voxel resolution. Segmented pores were labelled in AVIZO. Labelled pores were visualised in AVIZO (Fig. 3). Before analysing pore size, shape, orientation and location with respect to host clast, the data were binned to achieve a pixel size of 1.3 μm to give 1.3 x 1.3 x 1.3 μm^3 voxels and reduce the noise in the data. A total of 73 Ab1 SSMPs, with volumes over 6591 μm3 (3000 voxels) were identified for further analysis.

EDX analyses of minerals in the matrix and pores are compiled in **Supplemental Dataset S1**.
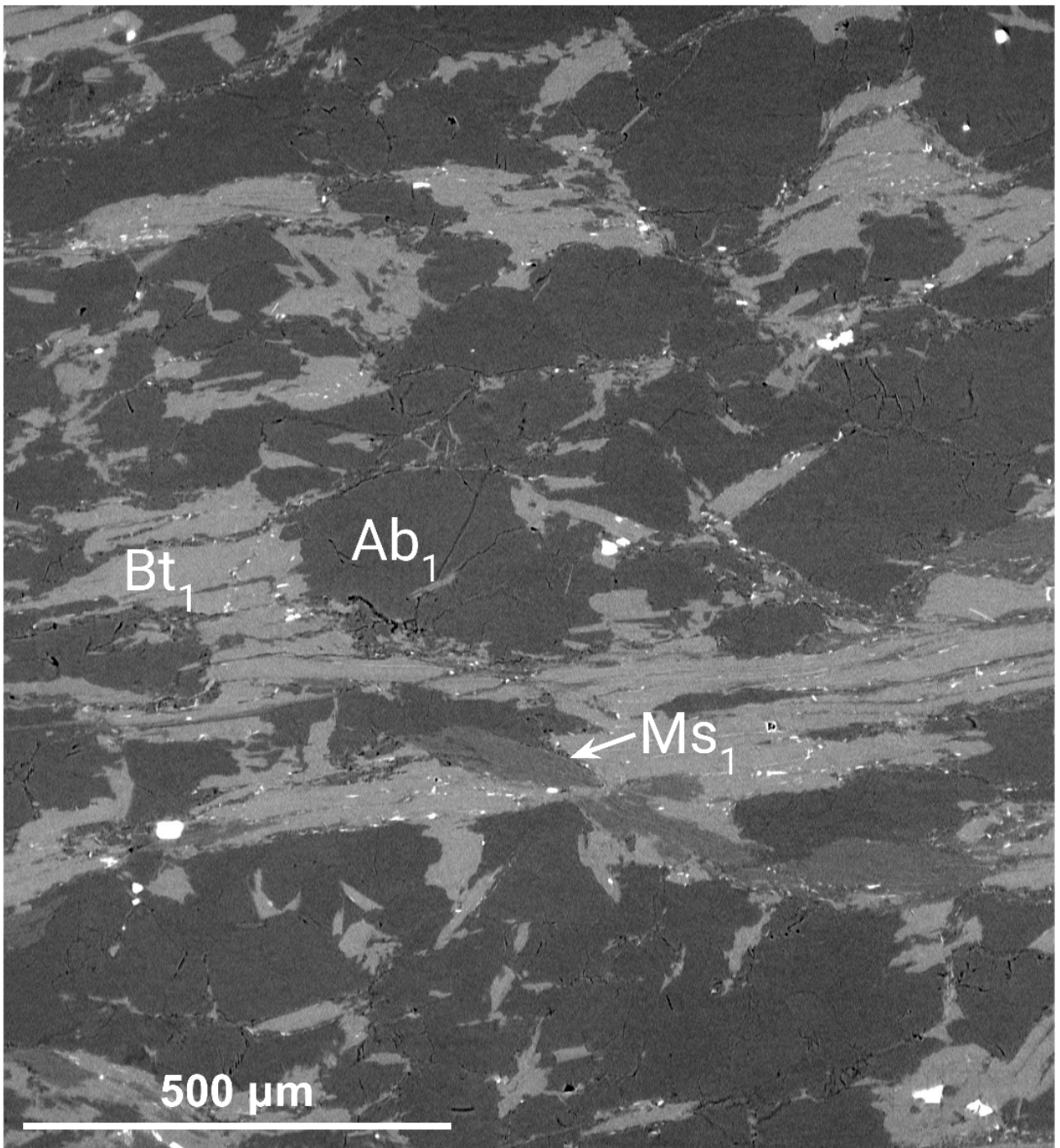
Suppl. Fig. 1 The non-sheared protolith to the ultramylonites investigated in this study. The image shows a virtual slice through a µCT dataset, grey values correspond to x-ray attenuation. The sample (CC12B) was collected just above the shear zone shown in Fig. 1b.
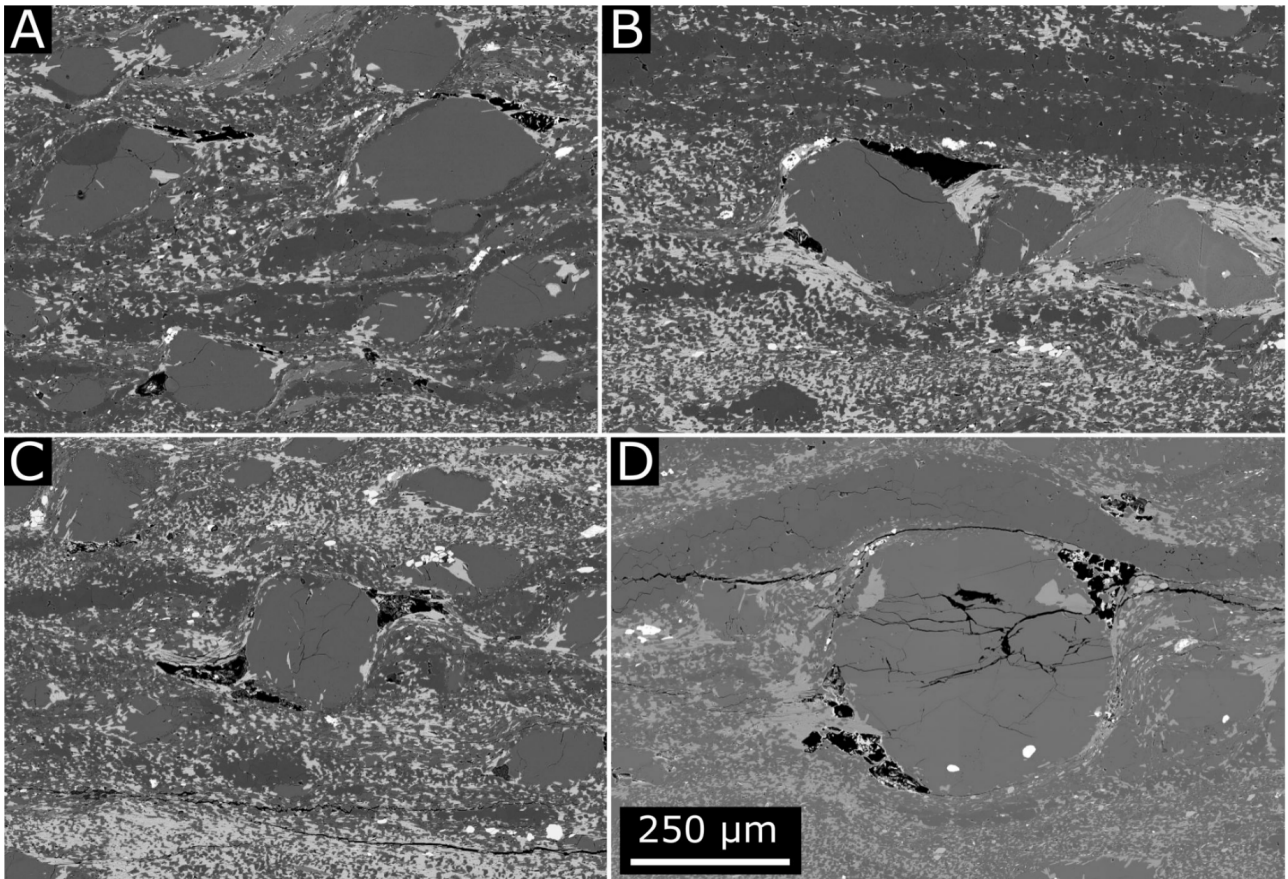
Suppl. Fig. 2 Electron images of Ab1 porphyroclasts of different morphologies and their associated

SSMPs. a-c) Backscatter electron images, d) Combined (50/50) backscatter/secondary electron

image. Scale bar applies to all images.
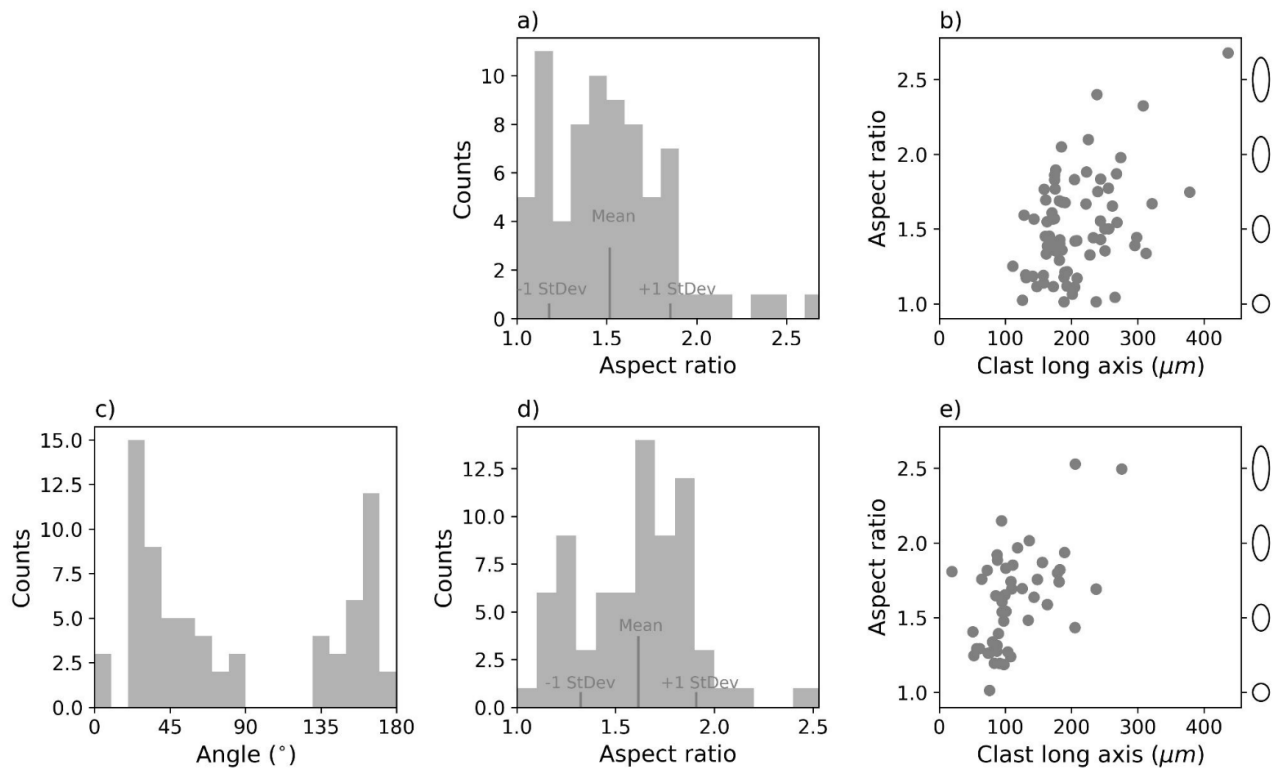
Suppl. Fig. 3 Aspect ratio, orientation and clast lengths ata from albite porphyroclasts in the undeformed metapsammite (a, b) and its mylonitised counterpart, which exhibits the SSMPs (c-e). In both cases, 73 clasts have been analysed.

Supplementary videos S1-4

Video S1 https://youtu.be/3s_fv-zFGUo This video shows an image slice that is migrating through our μCT volume. The image shows the x-ray attenuation of the least-attenuating voxel for each XY position along a 9.75 μm long ray path orthogonal to the image plane. This technique is excellently suited to highlight porosity in the sample, which appears black.

Video S2 https://youtu.be/R5Y7HFaRlYU This video shows a thick slice that migrates through a subvolume from a μCT dataset collected from an ultramylonite from the Cap de Creus, NE Spain. Pores have been segmented and labelled - individual pores are colour-coded, and only pores larger than 824 μm³ are shown. Note how pores occupy strain shadows around albite porphyroclasts. As the slide moves backwards through the volume, you see pores disappear that "fall out of" the thick slice at the front.

Video S3 https://youtu.be/AU2UeNvnMGw This video shows a thick slice that migrates through a subvolume from a μCT dataset collected from an ultramylonite from the Cap de Creus, NE Spain. Pores have been segmented and labelled - individual pores are colour-coded, and only pores larger than 824 μm³ are shown. Note how pores occupy strain shadows around albite porphyroclasts. As the slide moves backwards through the volume, you see pores disappear that "fall out of" the thick slice at the front.

Video S4 https://youtu.be/2j1sJDI8CYg This video shows a subvolume from a μCT dataset collected from an ultramylonite from the Cap de Creus, NE Spain. Pores have been segmented and labelled - individual pores are colour-coded, and only pores larger than 824 μm³ are shown. Note how pores occupy strain shadows around albite porphyroclasts.